JOURNAL OF GEOPHYSICAL RESEARCH, VOL. 104, NO. A11, PAGES 24,625–24,637, NOVEMBER 1, 1999

Coordinated incoherent scatter radar study of the January 1997 storm

M. J. Buonsanto,[1] S. A. González,[2] G. Lu,[3] B. W. Reinisch,[4] and J. P. Thayer[5]

Abstract. We describe many important features of the ionospheric *F* region as observed by the Sondrestrom, Millstone Hill, and Arecibo incoherent scatter radars (ISRs) and the Millstone Hill and Ramey Digisondes during January 6–10, 1997, with emphasis on the January 10, 1997 storm. Coordinated analysis of the data provides evidence for traveling atmospheric disturbances (TADs) and for two likely electric field penetration events linking these stations. Large and rapid changes in hmF_2 were seen at Arecibo and nearby Ramey which are related to the TADs and penetrating electric fields. Results are compared with simulations by the thermosphere-ionosphere electrodynamics general circulation model (TIEGCM), which utilizes high-latitude inputs given by the assimilative mapping of ionospheric electrodynamics (AMIE) technique. An important result of this study is that the TIEGCM is able to predict TADs similar to those observed. Exceptional features observed during this storm at Millstone Hill are a very large nighttime T_e enhancement on January 10 and a larger decrease in NmF_2 than predicted by the TIEGCM throughout the storm period. The latter appears to be related to an underestimation of the neutral temperature by the model.

1. Introduction

The chain of incoherent scatter radars (ISRs) near the 75°W meridian supported by the U.S. National Science Foundation (NSF) provides comprehensive measurements of ionosphere and thermosphere parameters which can be used to characterize the effects of geomagnetic storms on the Earth's upper atmosphere from the auroral zone to the equator.

Previous work with the ISRs [*Fejer et al.* 1990a, b; *Gonzales et al.*, 1983; Pi et al., Dynamical effects of geomagnetic storms and substorms in the middle latitude ionosphere: An observational campaign, submitted to *Journal of Geophysical Research*, 1998] has shown the penetration of magnetospheric electric fields from high to low latitude. *Fejer and Scherliess* [1995] introduced a technique to distinguish two types of electric field perturbations observed at Jicamarca, near the magnetic equator, during geomagnetically disturbed periods. These are prompt penetration magnetospheric convection electric fields and disturbance dynamo electric field perturbations caused by disturbed winds.

High-latitude enhancements in Joule heating expand the neutral atmosphere, launching traveling atmospheric disturbances (TADs) which can penetrate all the way to the equator and into the opposite hemisphere [*Fuller-Rowell et al.*, 1994]. These occur preferentially at night when the equatorward winds are reinforced by ion drag due to antisunward magnetospheric convection **ExB** ion drifts. Such equatorward surges in the neutral meridional wind are frequently observed by ISRs during major storms [e.g., *Babcock and Evans*, 1979; *Buonsanto et al.*, 1992].

Recently, *Buonsanto et al.* [1999] have used the ISR chain in a comprehensive study of the May 2–5, 1995, storm. That study identified three intervals of likely penetration of magnetospheric electric fields from high to low latitude. Unusual storm effects found were strong daytime equatorward wind surges, dusk effect evening enhancements in NmF_2 seen on three successive days at Millstone Hill, and an equatorward expansion of the equatorial anomaly zone as seen in GPS TEC data, apparently due to a strong upward plasma drift at the equator at Jicamarca, which led to a large increase in F_2 peak electron concentration NmF_2 at Arecibo.

In the present work, we carry out an ISR chain study of the January 10–11, 1997, storm using ISR data from the Sondrestrom facility in Kangerlussuaq, Greenland (67°N geographic latitude, 73°N geomagnetic latitude), Millstone Hill Observatory (42.6°N geographic latitude, 53°N geomagnetic latitude), and Arecibo Observatory (18.3°N geographic latitude, 29°N geomagnetic latitude). Unfortunately, Jicamarca ion drifts are not available during the periods of interest as only limited velocity data can be obtained from the Faraday double pulse mode used during this experiment (W. Swartz, private communication, 1997). We also include data from the Digisondes at Millstone Hill and at Ramey (18.5°N), near Arecibo. Owing to the offset between the geographic and geomagnetic poles, the ISRs at Sondrestrom, Millstone Hill, and Arecibo lie at high geomagnetic latitudes relative to their geographic locations. Sondrestrom lies along the auroral zone/polar cap boundary. Millstone Hill is a midlatitude site with an L value of 3, but it may be considered subauroral during geomagnetic storm conditions when it lies near the plasmapause boundary. Arecibo lies at lower midlatitudes, normally well poleward of the equatorial anomaly electron density peaks. Simultaneous *F* region measurements from the 3 ISRs and results from the global Thermosphere-Ionosphere Electrodynamics General Circulation Model (TIEGCM) reported here illustrate the prompt penetration of magnetospheric convection electric fields and the propagation of traveling atmospheric disturbances to low latitude.

[1]Massachusetts Institute of Technology, Haystack Observatory, Westford.
[2]Arecibo Observatory, Arecibo, Puerto Rico.
[3]High Altitude Observatory, National Center for Atmospheric Research, Boulder, Colorado.
[4]Center for Atmospheric Research, University of Massachusetts Lowell, Lowell.
[5]Geoscience and Engineering Center, SRI International, Menlo Park, California.

Paper number 1999JA900358.
0148-0227/99/1999JA900358$09.00

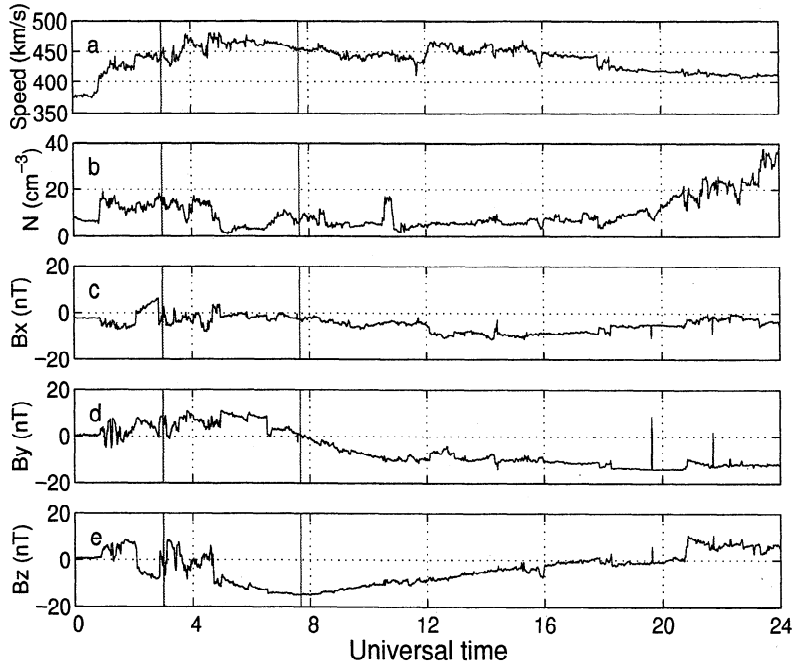

Figure 1. (a) Solar wind speed, (b) density, and (c-e) interplanetary magnetic field data from the Wind satellite for January 10, 1997. The vertical lines indicate times of possible electric field penetration events (see text).

The January 10–11, 1997, magnetic cloud event has been studied in detail by the International Solar-Terrestrial Physics (ISTP) community [*Fox et al.*, 1998]. Because of the excellent data coverage of this event, it has been also been chosen as an interval for coordinated analysis by the CEDAR Storm Study working group [*Buonsanto et al.*, 1997b].

2. Solar-Geophysical Conditions

Solar wind speed and plasma density data from the Wind satellite for January 10, 1997 are shown in Figures 1a and 1b. Interplanetary magnetic field (IMF) data from the Wind satellite for the same interval are shown in the lower three panels (in GSM coordinates). The geoeffectiveness (ability to produce geomagnetic disturbances) of three magnetic clouds, including the one which impacted the magnetosphere on January 10, 1997, have been studied by *Farrugia et al.* [1998]. Wind observed the passage of an interplanetary shock at ≈ 0052 UT followed by a ~4 hour period of high solar wind dynamic pressure. The arrival of the magnetic cloud at Wind was marked by a sharp southward turning of the IMF at 0442 UT. The minimum B_z = -15 nT at 0730 UT was followed by an extended period of gradual increase of B_z. The IMF in the cloud rotated nearly steadily with the total field B fairly constant as B_y decreased in tandem with the B_z increase. At 0800 UT, the satellite was located at X_{se}=87.6 R_e, and the solar wind velocity component V_x was -452 m s^{-1}, giving a ~20 min delay to the ionosphere. The solid vertical lines in Figure 1 mark times of likely electric field penetration events at the ISR sites as discussed below.

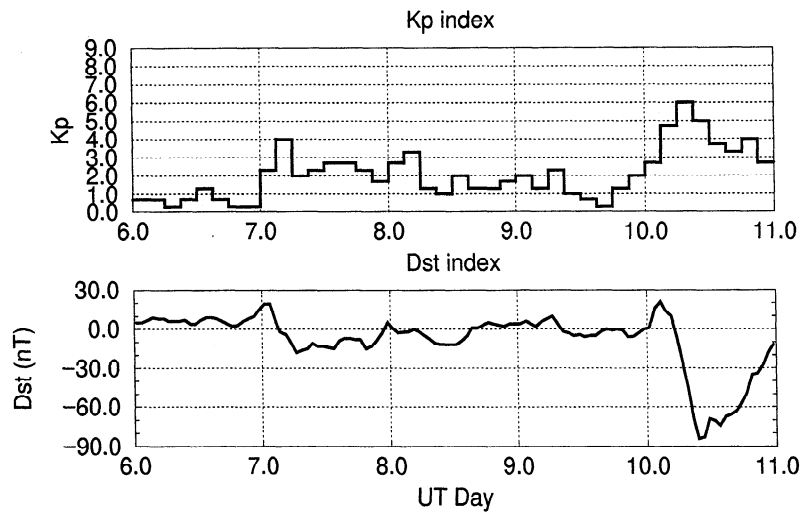

Figure 2. Geomagnetic indices *Kp* and *Dst* for January 6–10, 1997. *Kp* reached 6 and *Dst* reached a minimum value of -84 nT during the period of strong southward IMF (0600–1000 UT) on January 10.

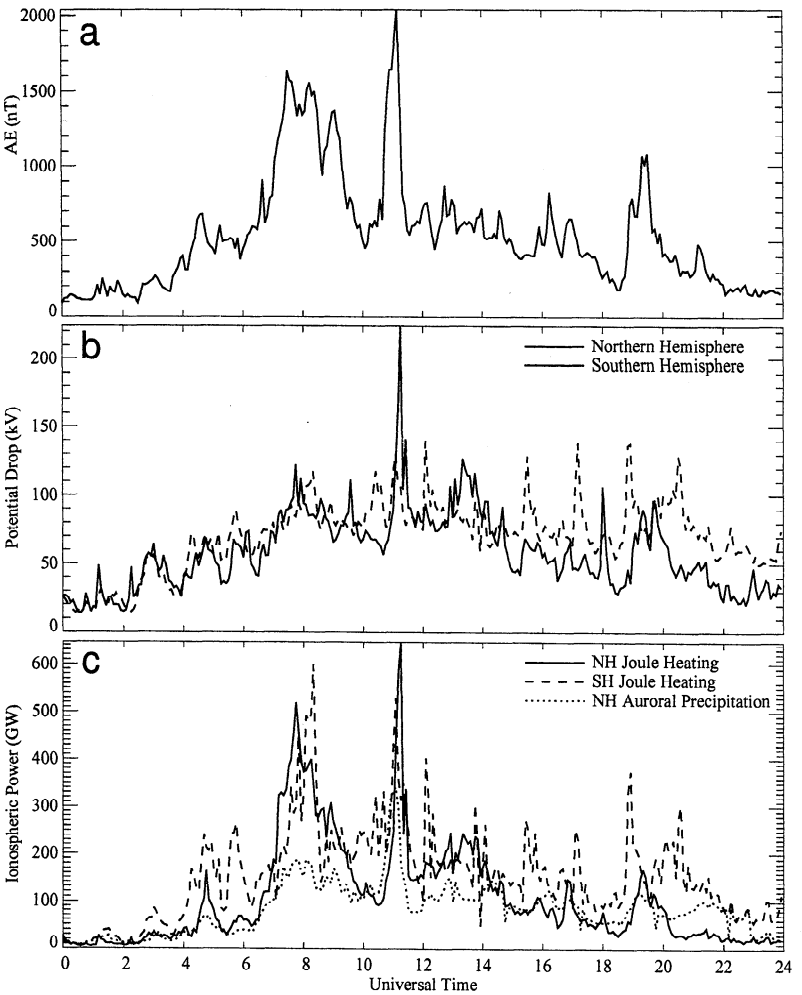

Figure 3. AMIE parameters characterizing the high latitude energy inputs on January 10, 1997. (a) The *AE*(68) index from 68 high-latitude magnetometer stations. (b) The cross polar cap potential drop, (c) AMIE Joule heating rates and auroral precipitation.

Figure 2 shows the *Kp* and *Dst* indices for January 6–10, 1997. *Dst* reached a minimum value of -84 nT in the interval 0900–1000 UT on January 10. *Kp* reached 6 during 0600–0900 UT. Geomagnetic storm commencements were observed at 15 stations near in the interval 0100–0115 UT on January 10 [*Coffey*, 1997].

3. The AMIE/TIEGCM

The TIEGCM, which was described by *Richmond et al.* [1992], is well-suited for the current study which deals with the *F* region/upper thermosphere. It uses a 5°x5° latitude-longitude grid and models the ionosphere and thermosphere self-consistently. In addition, it includes self-consistent calculation of winds and electric fields, i.e., the winds produce electric fields on closed field lines by dynamo action. These in turn modify the ion drag on the winds. In the present work, the auroral particle precipitation and magnetospheric convection electric fields are taken from the Assimilative Mapping of Ionospheric Electrodynamics (AMIE) technique [*Richmond and Kamide*, 1988; *Richmond et al.*, 1988]. The TIEGCM run covered the period 0000 UT on January 9 to 2400 UT on January 11, 1997. Recently, the TIEGCM with AMIE input has been used to study specific storm periods [*Buonsanto et al.*, 1997a; *Fesen et al.*, 1997; *Lu et al.*, 1998b].

Results from AMIE for the January 10–11, 1997, storm have been presented by *Lu et al.* [1998a]. Data used in the analysis included DMSP satellite ion drift and auroral precipitation measurements, NOAA satellite auroral precipitation observations, auroral UVI images from the Polar satellite, ion drift data from 6 SuperDARN radars and from the Sondrestrom and Millstone Hill ISRs, and data from 119 ground magnetometers. Figure 3 shows important parameters which characterize the high-latitude energy inputs on January 10. Figure 3a shows the *AE*(68) index calculated from magnetometer observations at 68 stations between 55° and 76° magnetic latitudes in the northern and southern hemispheres. Figure 3b shows the cross polar cap potential drop in the northern and southern hemispheres, and Figure 3c shows the Joule heating rates and auroral precipitation derived from AMIE. The largest geomagnetic activity (*AE*) and Joule heating rates occur near 0800 and 1100 UT during the prolonged interval of strongly southward IMF. These peaks in Joule heating launch TADs in the TIEGCM as discussed below.

4. Incoherent Scatter Radar Data

January 6–10, 1997, was an incoherent scatter coordinated observation interval dedicated to support of campaigns known as the

mesosphere lower-thermosphere coupling study (MLTCS) and the coupling and dynamics of the ionosphere-thermosphere system (CADITS). These campaigns both emphasize detailed local measurements, i.e., observations above and in the vicinity of the observing stations. Sondrestrom data were taken in three positions: (1) azimuth 141°, elevation 80° (directed along the magnetic field line); (2) azimuth 261°, elevation 70°; and (3) azimuth 21°, elevation 70°, using both long pulse and alternating code transmit modes. Each position was integrated for 5 min with a total cycle time of 17 min including antenna motion. Millstone Hill daytime (≅ 0700–1800 LT) measurements were taken in six positions, four at the cardinal points at an elevation angle of 45°, one at the zenith, and one up the magnetic field line. Use of both alternating code and long pulse modes provided the altitude resolution needed for E region studies at the expense of a long cycle time (44 min). Each night (≅ 1830–0700 LT) during January 6–9 a local 10-position experiment was run using long pulses only with a 35-min cycle time. Arecibo data were taken in the zenith-pointing position and at night only owing to an upgrade in progress at the facility. These provided excellent 1-min time resolution.

4.1. Ion drifts on January 10 at the Three Incoherent Scatter Radar Sites

For Sondrestrom and Millstone Hill, measurements in three or more directions are used to estimate the three-dimensional ion velocity vector above each site, using the assumption that the measurements are sampling a uniform ion velocity field. Figure 4 shows the component of the ion drift vector perpendicular to the Earth's magnetic field, positive northward and upward ($V_{\perp N}$) as seen by the Sondrestrom and Millstone Hill ISRs. The magnetic inclination angle is ≅ 70° at Millstone Hill and ≅ 80° at Sondrestrom. Figure 4 also shows the upward ion drift at Arecibo. $V_{\perp N}$ represents the **ExB** plasma drift due to an eastward electric field. Figure 4a shows $V_{\perp N}$ at Sondrestrom determined from radar measurements of resolved F region ion velocities by assuming the ions above 180 km are **ExB** drifting and by applying a weighted averaging scheme to the data. The weighted average included data from 180 to 400 km altitude after excluding data with drift errors in excess of 400 m s^{-1}. Figure 4b shows $V_{\perp N}$ at 300 km above Millstone Hill obtained from line-of-sight ion velocity data above 44° elevation angle in the altitude range 240–360 km. The vertical (upward) ion drift velocities at Arecibo shown in Figure 4c are height-averages of line-of-sight velocity measurements from altitudes 250–400 km. The vertical ion drifts may be considered as a sum of components in the magnetic meridian parallel and perpendicular to **B** as they are influenced by effects of neutral winds as well as east-west electric fields.

Strong ion drifts (> 1000 m s^{-1}) are observed at Sondrestrom, but not at the lower-latitude stations, suggesting that the magnetospheric convection electric fields were generally confined to latitudes poleward of Millstone Hill. However, two electric field penetration events were identified as described below. The eastward component of the ion drift $V_{\perp E}$ at Millstone Hill (not shown) was of comparable magnitude to $V_{\perp N}$.

The solid vertical lines in Figure 4 indicate the times of possible electric field penetration events. The first event occurred at 0300 UT. B_z turned northward at 0252 UT suggesting a time lag ~ 8 min to the ionosphere, which, considering the X_{se} position of the Wind satellite (see above), is shorter than necessary to relate the B_z change to the ionospheric electric field effects. However, the Y_{se} position of the Wind satellite (Y_{se}=-59 R_e) means that differences in the ambient solar wind magnetic field between that at the position of the satellite and that at an equal X distance directly in front of the magnetopause may be responsible for the insufficient time lag. Unfortunately, IMP 8 data which could elucidate this question are not available at this time. A decrease in the **ExB** plasma drift component $V_{\perp N}$ as seen at 0300 UT (corresponding to ≈ 2200 LT at Millstone Hill and 2300 LT at Arecibo) is due to a westward electric

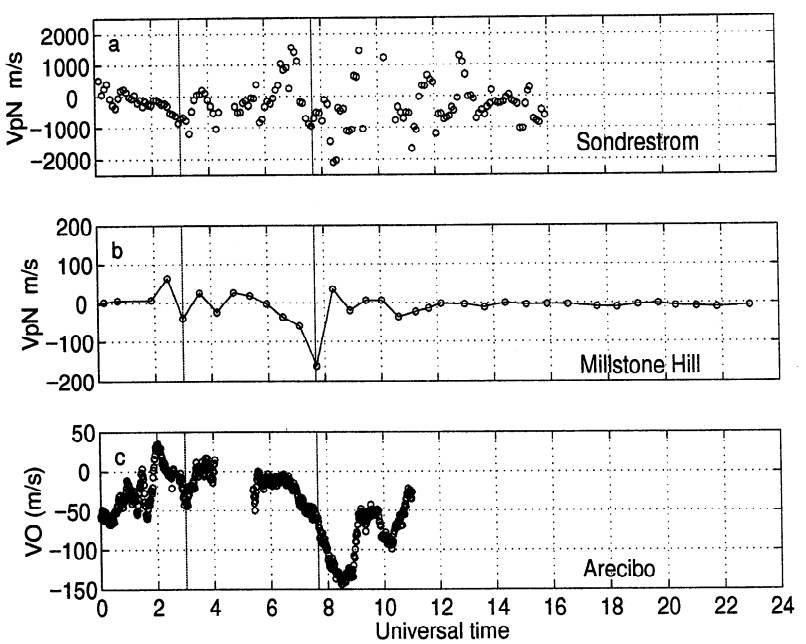

Figure 4. Northward and/or upward ion drifts on January 10, 1997 at the three incoherent scatter radar sites, showing effects of an eastward electric field: (a) Sondrestrom, (b) Millstone Hill, (c) Arecibo. The vertical lines indicate times of likely penetration of a magnetospheric electric field from high to low latitudes. The first event (0300 UT) may have been associated with a northward turning of the IMF observed by Wind at 0252 UT. The second event (0740 UT) occurred during a period of strong and nearly steady southward IMF (Figure 1).

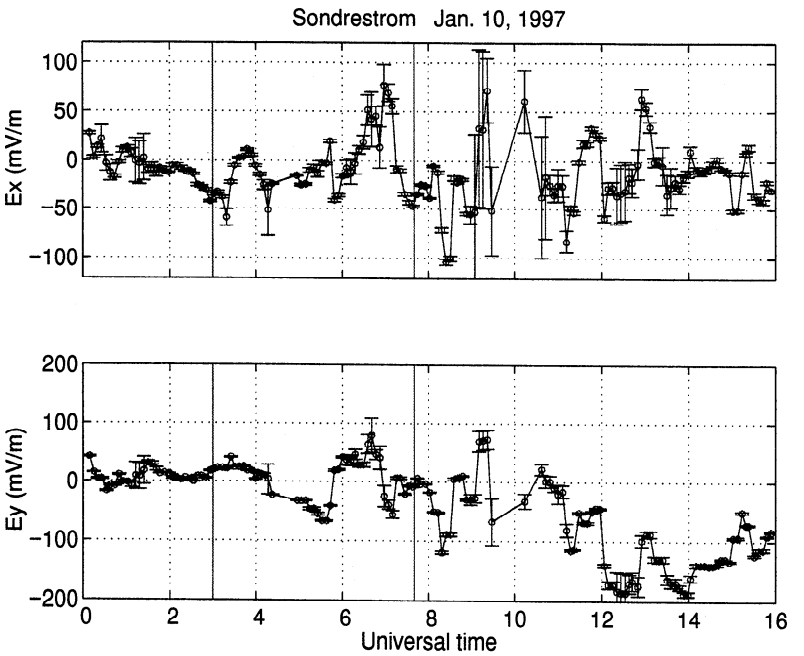

Figure 5. Eastward (E_x) and northward (E_y) electric fields as measured by the Sondrestrom ISR on January 10, 1997. The electric field structure is a result of storm time variability and the radar sampling of different parts of the ion convection pattern with time. The vertical lines indicate times of possible electric field penetration events (see text).

field. Work by *Gonzales et al.* [1983], *Sastri et al.* [1992] and others shows that in the premidnight sector, a sudden increase in IMF B_z results in penetration of a westward electric field to low latitudes.

The second of the two electric field penetration events (0740 UT) does not have an apparent IMF trigger but corresponds to strong and steady southward B_z as shown in Figure 1 at 0700–0800 UT and strong geomagnetic disturbances as seen in *Dst* (Figure 2), and a peak (though a larger peak occurred near 1100 UT) in the *AE* index, cross polar cap potential drop, and Northern Hemisphere Joule heating as determined by AMIE (Figure 3). *Fejer* [1997] has shown that in this local time sector (~0300 LT) the expected response to a rapid increase in cross polar cap potential drop at Arecibo is penetration of a westward electric field, giving a downward drift.

4.2. Sondrestrom Data

The Sondrestrom radar-derived electric field estimates from 0000 to 1600 UT on January 10, 1997 are displayed in Figure 5 in eastward (E_x) and perpendicular northward (E_y) components. Significant electric field structure is observed throughout the interval shown, with the vertical lines identifying times of possible electric field penetration events, based on the lower-latitude observations as in Figure 4. The electric field structure is a result of storm time variability and the radar sampling of different parts of the ion convection pattern with time. During the time of the first electric field penetration event, Sondrestrom was located near magnetic midnight experiencing westward electric fields or, for this time, antisunward ion drifts. The electric field was moderately strong at this time reaching levels of ≈45 mV m^{-1}. During the time of the second electric field penetration event, Sondrestrom was in the auroral zone and measuring westward electric fields of ≈50 mV m^{-1}. The moderate southward ion convection at this time placed the measurements just below the dawn cell convection reversal boundary. However, by 0815 UT the electric field intensified to 140 mV m^{-1} and rotated towards the south. This produced sunward convection during this time as the radar made measurements along the equatorward side of the dawn cell. During this time, strong Joule heating rates were determined by the radar, as described by *Sanchez et al.* [1998], and maximum enhancements in electric current over western Greenland were observed between ~0800 and 0830 UT.

For ~ 2 hours after 0900 UT, Sondrestrom was sampling the low-density polar cap resulting in generally poor signal statistics. From 1100 to 1200 UT, the electric field rotated from westward to southward indicating that the site was again transitioning to the equatorward side of the convection reversal, and beginning to sample the dawn cell return flow. After 1200 UT, the electric field remained mostly southward and of strong magnitude, resulting in large eastward ion convection (~3 km s^{-1}). Over this period, the eastward convection extended well into the postnoon sector reflecting the strong B_y negative conditions of the IMF during this time. A DMSP-F12 pass at 1443 UT confirms the large eastward convective flow at the magnetic latitude of Sondrestrom (M. R. Hairston, private communication, 1998).

4.3. Millstone Hill Data

Figure 6 shows NmF_2 from the Millstone Hill ISR compared to results from the TIEGCM. The data prior to the storm exhibit anomalous nighttime increases in NmF_2. These are the subject of a separate paper by *Mikhailov and Förster* [1999]. The effect of the storm is a major depletion in NmF_2 on the last day of the experiment (January 10), both at night and during the daytime. Numerous experimental and theoretical studies show that decreases in NmF_2 during storms result from neutral composition changes, i.e., decreases in the ratio of O concentration to the concentration of N_2 and O_2. However, it is believed that the neutral composition disturbance zone which causes these negative storm effects, i.e., decreases in NmF_2, is normally confined to higher latitudes in winter than in summer by the prevailing summer to winter neutral wind flow. For example, simulations by the Coupled Thermosphere Ion-

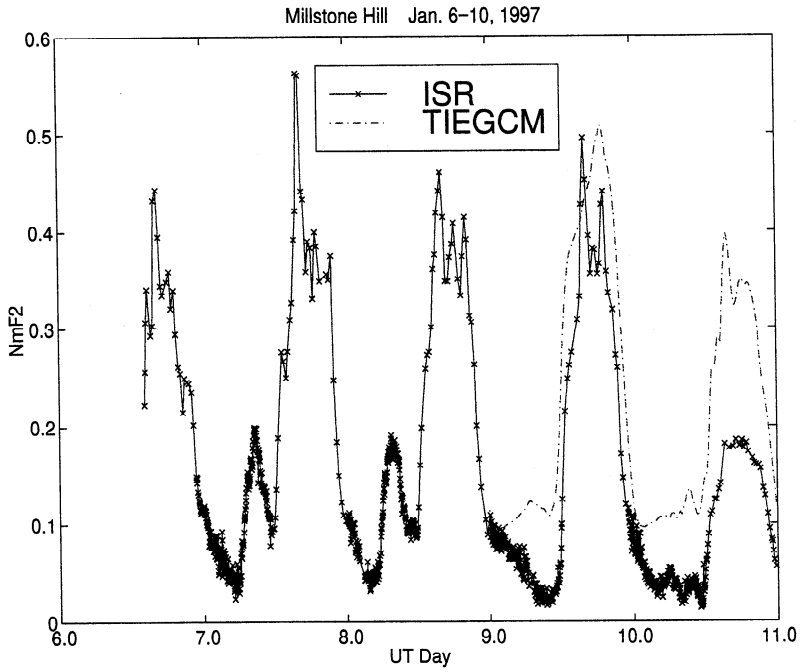

Figure 6. NmF_2 from the ISR and the TIEGCM at Millstone Hill for January 6–10, 1997. The main effect of the storm on January 10 is a strong depletion in NmF_2. The TIEGCM also predicts a decrease, but a smaller one than is observed.

osphere Model (CTIM) show that Millstone Hill should experience a long-lived decrease in mean molecular mass during a winter storm accompanied by an increase in NmF_2 [*Fuller-Rowell et al.*, 1996]. NmF_2 from the TIEGCM shows little effect of the storm during the night of January 10 compared to the preceding quiet nights, and a decrease during the following day compared to the previous quiet days. However, the TIEGCM predicts a small decrease while the observations show a large decrease. The decrease in NmF_2 on January 10 may be explained by the local time of this storm commencement (0100 UT = 2000 LT at 75°W). *Titheridge and Buonsanto* [1988] showed that storms which commence during the nighttime hours at a northern hemisphere winter station (Stanford) showed a negative response in TEC throughout the following day, as found in our data from January 10, 1997. Model simulations for equinox conditions by *Fuller-Rowell et al.* [1994] also illustrate the importance of the local time of storm onset in determining the electron density response.

Figures 7a and 7b show Millstone Hill NmF_2 and F_2 peak height

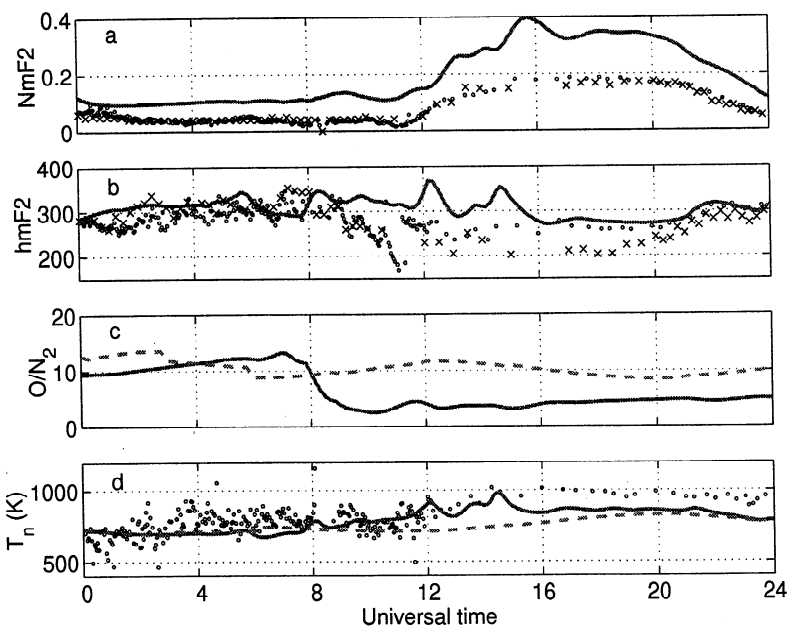

Figure 7. Important parameters above Millstone Hill on January 10, 1997: (a) NmF_2 and (b) hmF_2 observed by the ISR (circles) and the Digisonde (crosses) and predicted by the TIEGCM (solid line). (c) The ratio of neutral atomic oxygen density to molecular nitrogen density at 300 km altitude from the TIEGCM (solid line) and the MSIS-86 model (dashed line). (d) The neutral temperature at 300 km observed by the ISR (circles) and predicted by the TIEGCM (solid line) and the MSIS-86 model (dashed line).

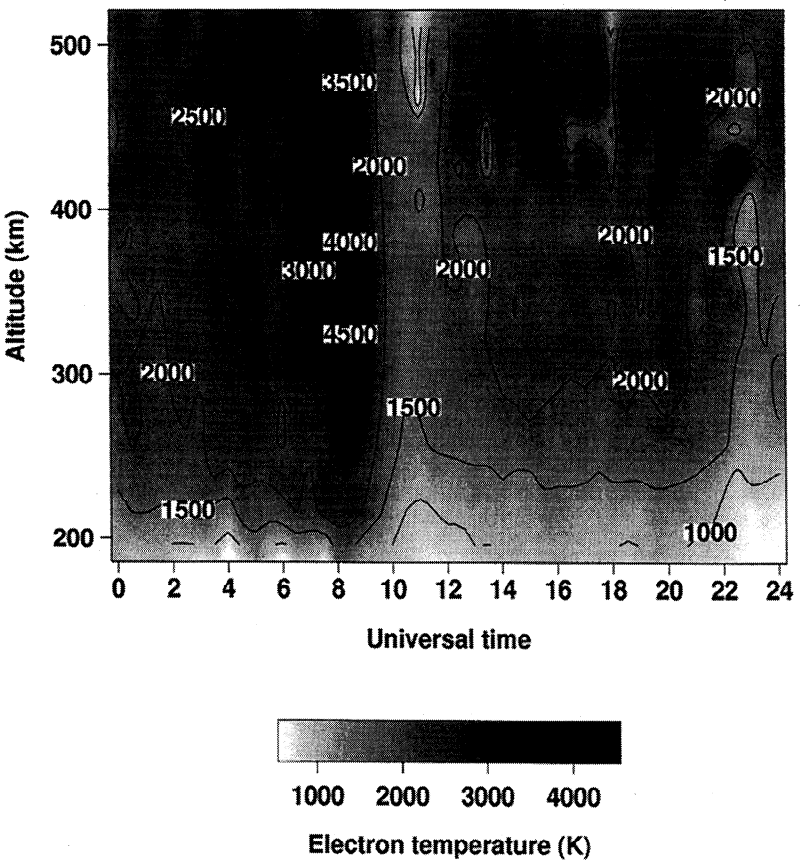

Figure 8. Electron temperature (T_e) measured by the Millstone Hill ISR on January 10, 1997. Nighttime T_e exceeds that during the day, and an especially strong enhancement is seen at 0800 UT (0300 LT).

(hmF_2) for January 10, 1997, from the ISR zenith antenna, the Digisonde, and the TIEGCM. Digisonde NmF_2 and hmF_2 are obtained from electron density (N_e) profiles determined from inversion of ionogram traces using the technique of *Reinisch and Huang* [1983] and *Huang and Reinisch* [1996]. This technique has been validated by comparison with ISR data at Millstone Hill and Arecibo [*Chen*, 1997].

Both the ISR and the Digisonde data show that NmF_2 was extremely low during the nighttime hours compared to the preceding geomagnetically quiet nights. This reduces the signal-to-noise ratio, increasing the uncertainty in the ISR derived N_e; this may account for the scatter in the ISR hmF_2 as shown in the Figure 7. According to the ISR data, hmF_2 undergoes a sharp drop just before sunrise for a brief period, apparently associated with a molecular ion layer. The observed NmF_2 is also lowest at this time, i.e., the O^+ density is extremely low so that most of the residual ionization is composed of molecular ions below 200 km. This is a common occurrence during ionospheric storms at Millstone Hill [e.g., *Buonsanto et al.*, 1992; *Buonsanto*, 1995]. The low electron densities probably correspond to an electron density trough, but as the ISR experiment did not include elevation scans, we do not have data providing the latitude variation of NmF_2 which would show the trough. There is too much uncertainty in the Digisonde data to determine hmF_2 at this time.

A depletion in NmF_2 in the hours before sunrise during storms appears in "AC/DC" analysis of ionosonde data [*Rodger et al.*, 1989; *Field and Rishbeth*, 1997] at midlatitudes for all seasons. It is explained by a composition disturbance zone which is first advected from high to midlatitudes at night due to enhanced equatorward neutral winds, and subsequently rotates into the dawn sector [*Prölss*, 1993]. Increased densities of N_2 and O_2 increase the rate of conversion of O^+ ions to the molecular ions NO^+ and O_2^+.

During the following day time period the Digisonde hmF_2 is systematically lower than the ISR hmF_2 (by ≈ 55 km at 1700–1800 UT). The differences between the ISR and the Digisonde hmF_2 may be due to three different causes. (1) The ISR beam width is only 1°, which illuminates an area of the sky 5 km in diameter at 300 km altitude. However, the Digisonde beam width is ≈ 45° at this frequency which means that the beam illuminates an area of the sky a few hundred kilometer on a side, so if the F_2 region is nonuniformly stratified, the two instruments may measure a different value for hmF_2. (2) If the F_2 peak region of the electron density profile is structured, i.e., does not have a smooth parabolic shape but has more than one peak, the Digisonde will find the lowest peak to be hmF_2, whereas the ISR will average through the entire region and so will arrive at a higher value for hmF_2. *Chen et al.* [1994] found ISR hmF_2 larger than Digisonde hmF_2 by 4–17 km, depending on the profile thickness in coordinated analysis of data from Millstone Hill collected during four months in 1990 and attributed the difference to this cause. (3) Unpublished comparisons between Millstone Hill ISR data obtained using different pulse lengths suggests that range smearing of the daytime 410-μs pulse length ISR data used here can account for ≈ 5 km of the ISR-Digisonde hmF_2 difference.

The solid lines in Figure 7 shows results from the TIEGCM on this day. The model NmF_2 is larger than the measured NmF_2, with the largest percentage difference between the model and the data at night. Figure 7c shows the O/N_2 ratio at 300 km altitude from the TIEGCM compared to that predicted by the MSIS-86 model. O/N_2

from the TIEGCM is up to a factor of 2 or more smaller than O/N_2 from MSIS-86 after 0800 UT. Figure 7d shows the neutral temperature (T_n) at 300 km from the TIEGCM, MSIS-86, and the ISR. T_n is determined from the Millstone ISR data using a heat balance calculation [*Bauer et al.*, 1970; *Alcayde et al.*, 1982]. The technique as currently applied at Millstone Hill has been recently described by *Buonsanto and Pohlman* [1998]. T_n from the TIEGCM agrees well with T_n from MSIS-86 prior to 0800 UT, but T_n from the TIEGCM is larger than T_n from MSIS-86 after 0800 UT. The ISR T_n is larger than that predicted by both the TIEGCM and MSIS-86 during most of January 10. A change in T_n modifies the scale heights of the neutral constituents, and a larger T_n should decrease the atomic to molecular neutral composition ratio [e.g., *Richards and Wilkinson*, 1998]. This can explain why O/N_2 is smaller in the TIEGCM than in MSIS-86 after 0800 UT. The even larger ISR T_n during most of January 10 suggests that O/N_2 should be even smaller than predicted by the TIEGCM. This would decrease NmF_2 by decreasing the rate of production of O^+ (daytime) as well as increasing the recombination rate (day and night). Increases in T_n and ion temperature (T_i) also increase the $O^+ + N_2$ and $O^+ + O_2$ reaction rates directly and high electron temperatures (Figure 8) increase the recombination rate of electrons. Such decreases in O/N_2 and increases in temperatures can explain why the measured NmF_2 is smaller than that predicted by the TIEGCM. From a comparison between observed NmF_2 and their theoretical calculations, *Mikhailov and Förster* [1999] concluded that the O/N_2 ratio was less by a factor 3.7 compared to the MSIS-86 predictions on January 10.

Figure 8 shows Millstone Hill T_e for January 10, 1997. The T_e enhancement near 0800 UT, a time of rapidly decreasing *Dst* (Figure 2), has been described by *Foster et al.* [1997]. It is apparently due to downward conduction of heat from the magnetosphere, where the heat is generated by Coulomb collisions between ring current ions and electrons. This is one of the mechanisms proposed to explain SAR arcs [*Cole*, 1965; *Kozyra et al.*, 1987]. Unfortunately, no optical data are available above Millstone Hill on this night. The high nighttime T_e (0000–1000 UT = 1900–0500 LT) relative to the subsequent daytime period may be due to the low electron concentration which reduces the electron cooling rate, combined with the fact that the magnetically conjugate point is sunlit the entire night, providing an inflow of photoelectrons which heat the exosphere and thermosphere above Millstone Hill [*Evans*, 1967].

Figure 9 shows the horizontal neutral wind in the magnetic meridian (positive northward) above Millstone Hill for January 10. The solid line shows the winds obtained using all the ISR data above an elevation angle of 44°. The diamonds show the winds from the TIEGCM. The triangles show the winds from the ISR when only the position looking up the magnetic field line is used in the wind calculation. The circles show winds derived from the servo model [*Rishbeth*, 1967; *Rishbeth et al.*, 1978] using the Digisonde hmF_2, assuming the MSIS-86 neutral atmosphere and taking T_e and T_i equal to the MSIS-86 T_n values. The calculation only uses ISR data for the electric field correction needed by the servo model winds technique. The technique for deriving neutral meridional winds from the servo model [*Buonsanto*, 1986] was most recently described and compared with other wind-derivation methods by *Buonsanto et al.* [1997c]. The ISR winds are calculated using the method of *Salah and Holt* [1974]. The formula of *Pesnell et al.* [1993] is used for the O^+–O collision frequency for the ISR and servo model wind determinations and in the TIEGCM. Strong equatorward winds are seen during the interval 0700–0800 UT. The strong surge in the ISR winds which maximizes at 0722-0724 UT is apparently the signature of a TAD launched by intense Joule heat-

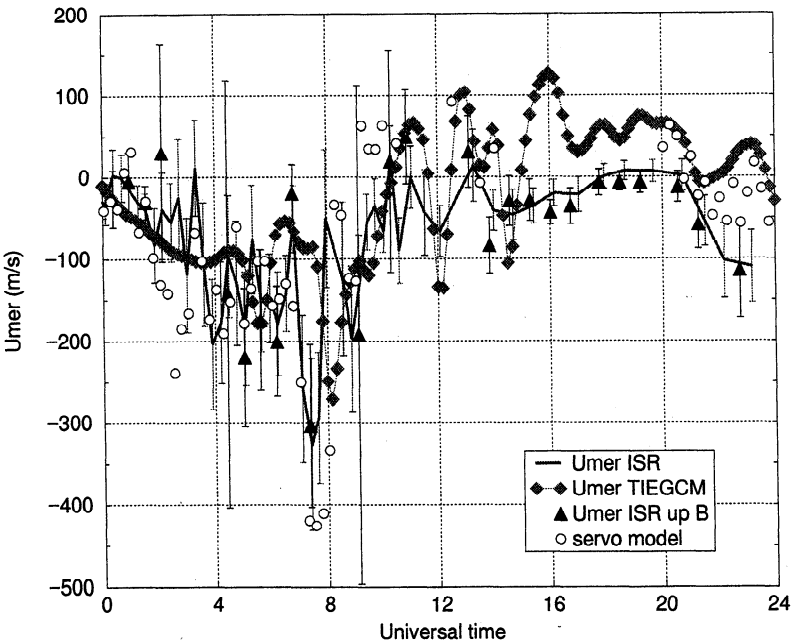

Figure 9. Neutral winds in the magnetic meridian (horizontal and positive northward) at Millstone Hill on January 10, 1997. Solid line indicates winds at 300 km altitude determined using ISR ion velocity measurements taken in 6 (day) and 10 (night) directions. Triangles indicate winds at 300 km altitude determined using ISR ion velocity measurements up the magnetic field line only. Circles indicate winds from the servo model at hmF_2. Diamonds indicate winds at 300 km altitude predicted by the TIEGCM.

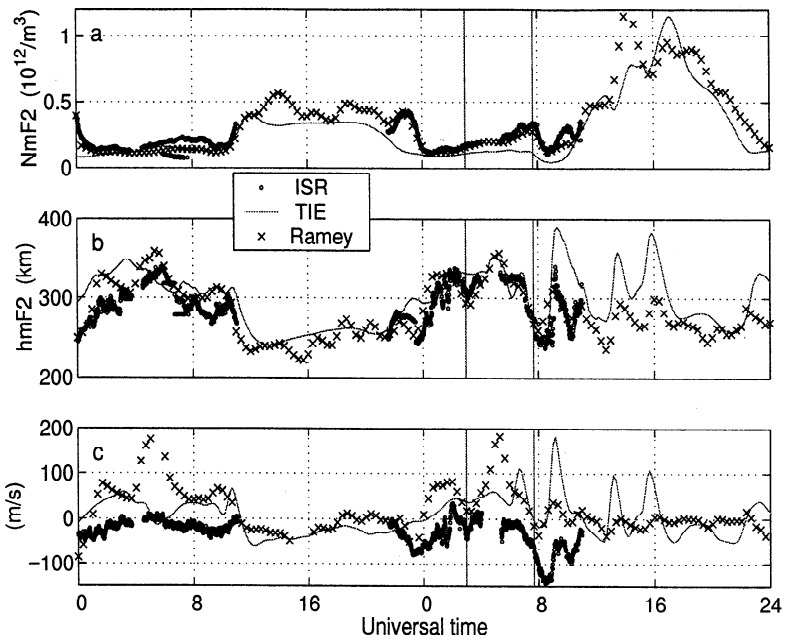

Figure 10. Important parameters above Arecibo and nearby Ramey, Puerto Rico on January 9–10, 1997. (a) NmF_2 and (b) hmF_2 observed by the Arecibo ISR (circles) and the Ramey Digisonde (crosses) and predicted by the TIEGCM (solid line). (c) Vertical ion velocity (average of data from 250–400 km altitude) observed by the ISR (circles) compared with winds in the magnetic meridian (positive southward) from the TIEGCM at 300 km altitude (solid line) and from the servo model at hmF_2 at Ramey (crosses) on January 9–10, 1997. The vertical lines indicate times of possible electric field penetration events (see text).

ing at high latitude. The servo model wind surge maximizes at 0730 UT. The time difference between the ISR and servo model wind surge maxima is apparently due to the temporal resolution of the data, 35 min for the ISR winds and 20 min for the Digisonde hmF_2. The TIEGCM also predicts a wind surge, but with a maximum at 0810 at Millstone Hill. Further evidence for this TAD is provided by the Arecibo data as shown below.

4.4. Arecibo Data

Figures 10a and 10b show NmF_2 and hmF_2 from the Arecibo ISR and from the nearby Ramey Digisonde for January 9–10, 1997, compared with the TIEGCM. NmF_2 from the two instruments agree well as they should, showing that the ISR data are well-calibrated. The observed NmF_2 is usually a little larger than that predicted by the TIEGCM. However, the TIEGCM reproduces the positive phase storm effect seen in the Ramey data on January 10. There is also good agreement between the times of the modeled and observed fluctuations in hmF_2 during the day on January 10, although the amplitudes of the hmF_2 fluctuations are larger in the model than in the data. As discussed further below, this is an important result of the present work, i.e., the TIEGCM, driven by realistic AMIE inputs, has been successful in predicting the timing of these hmF_2 fluctuations which are due to the passage of gravity waves.

The dip in hmF_2 at 0300 UT on January 10 corresponds to the electric field penetration event discussed earlier. The extended drop in hmF_2 between 0700 and 0900 UT on January 10 and the sudden jump in hmF_2 just after 0900 UT are discussed further below.

Figure 10c shows the observed vertical ion velocity at Arecibo (circles) compared with the neutral meridional wind from the TIEGCM at Arecibo (solid line) and the servo model at Ramey (crosses) for the night of January 9–10, 1997. The servo model winds are derived from the measured hmF_2 as done for Millstone Hill. Since the Arecibo ISR did not measure ion drifts in three or more directions needed to estimate electric fields during this experiment, the electric field correction needed by the servo model technique is estimated using the electric field model of *Richmond et al.* [1980]. This electric field model does not reproduce electric field disturbances which occur during disturbed periods due to prompt penetration electric fields or the disturbance dynamo, so some of the variations in the derived servo model winds are artifacts introduced by inadequate specification of the electric field correction.

The observed ion velocity in Figure 10, which is due to neutral winds, electric fields, and diffusion, is obtained by averaging ISR data in the altitude range 250–400 km. The neutral winds are in the magnetic meridian, positive southward, so they should be positively correlated with the vertical ion drifts. The TIEGCM winds are at an altitude of 300 km, while the servo model winds are at hmF_2. The neutral winds from both the TIEGCM and the servo model show TADs during the interval 0700–1700 UT which are generally in phase with the observed ion drift (when available). Such TADs strongly affect the vertical ion drift, and the consistency in the timing of the TADs as given by the TIEGCM winds, servo model winds, and the vertical ion drifts shows that the TIEGCM has managed to reproduce major fluctuations in the neutral winds above Arecibo on this night. *MacPherson et al.* [1998] have shown that the meridional neutral wind has a strong effect on the O^+–H^+ transition height (h_T) above Arecibo. On this night there is a dramatic collapse in h_T from 500 km at 0700 UT to 425 km at 0800–0830 UT (not shown in the Figure 10). At the same time, a strong downward drift and a poleward wind are seen which result in a large drop in hmF_2 to ~250 km. The low hmF_2 results in a large decrease in

NmF_2 due to enhanced recombination. The downward drift abates near 0900 and hmF_2, NmF_2, and h_T increase. The TIEGCM hmF_2 shows similar behavior, except that the hmF_2 increase at 0900 UT in the model is larger than in the data. As discussed below, both electric fields and neutral winds may be involved in causing the strong downward drift which maximizes at 0830 UT and the strong abatement at 0900 UT.

5. Discussion

The fall in hmF_2 and strong downward drift at Arecibo between 0800 and 0900 UT (Figure 10) appears to be similar to the midnight collapse of the Arecibo ionosphere which has been well documented [e.g., *Crary and Forbes*, 1986]. However, as it occurs at 0400–0500 LT, it seems unlikely that it could be exclusively due to tidal effects as proposed by Crary and Forbes. *Buonsanto and Foster* [1993] found a ~200 km drop in hmF_2 at Arecibo during the March 20–21, 1990, storm associated with abatement and reversal of a strong nighttime equatorward wind surge. The TIEGCM winds show an equatorward surge of 110 m s^{-1} at 0640 UT which appears to delay the postmidnight collapse, and the servo model shows equatorward winds of similar magnitude maximizing 1 hour 20 min earlier.

In their recent review, *Kelley and Miller* [1997] explain how when electric fields and neutral winds combine (see their equation 8) to produce a downward ion drift, this condition is unstable, i.e., there is no equilibrium; the ionosphere continuously falls as occurs during the postmidnight collapse at Arecibo. Unfortunately, because zenith data only were available, we cannot unambiguously separate effects of winds and electric fields from the Arecibo ISR data alone. However, we note the westward electric field penetration event at 0740 (Figure 4) which occurred during the interval of this strong downward drift and may have accelerated it. We identified this as an electric field penetration event because of the observed response at Sondrestrom and Millstone Hill and because prompt penetration electric fields are expected to produce a downward plasma drift at this local time. By contrast, a disturbance dynamo electric field would tend to give an upward drift at low latitude [*Fejer and Scherliess*, 1995].

The TIEGCM clearly shows a strong abatement in the equatorward wind associated with the strong downward ion drift (Figure 10). This abatement apparently occurs in the interval between two southward propagating TADs, the one with the smaller amplitude maximizing in the TIEGCM at 0640 UT and the one with the larger amplitude seen at 0900 UT. This latter TAD is apparently the one seen at Millstone Hill at ≈ 0723 UT (ISR) and ≈ 0730 (servo model). It causes a sharp reversal in the downward vertical drift velocity at Arecibo at 0900 UT. The servo model winds also clearly show a strong southward surge at 0900 UT. If this indeed is a TAD, it has a high-latitude source. Strong Joule heating is inferred from AMIE analysis, maximizing in the Northern Hemisphere at 0745 UT (Figure 3). At 0705 UT, AMIE shows the peak heating occurred at 70° apex magnetic latitude at the longitudes of Millstone Hill and Arecibo (Figure 11). Figure 11 is labeled corrected Joule heating as the AMIE calculation includes a term which accounts for the variability in the large-scale electric fields [*Lu et al.*, 1998a].

Figure 12 shows a difference plot of the neutral meridional wind (positive toward geographic north) from the TIEGCM at 70°W. This compares the TIEGCM winds on January 10, 1997, with those from a quiet day earlier in the same model run. Figure 12 clearly shows wind surges with high northern latitude source regions penetrating from high to low latitudes and well into the southern hemisphere. Weak TADs are seen propagating northward from high southern latitudes. These are weak due to the dissipative effects of greater ion drag in the summer hemisphere. Similar effects were

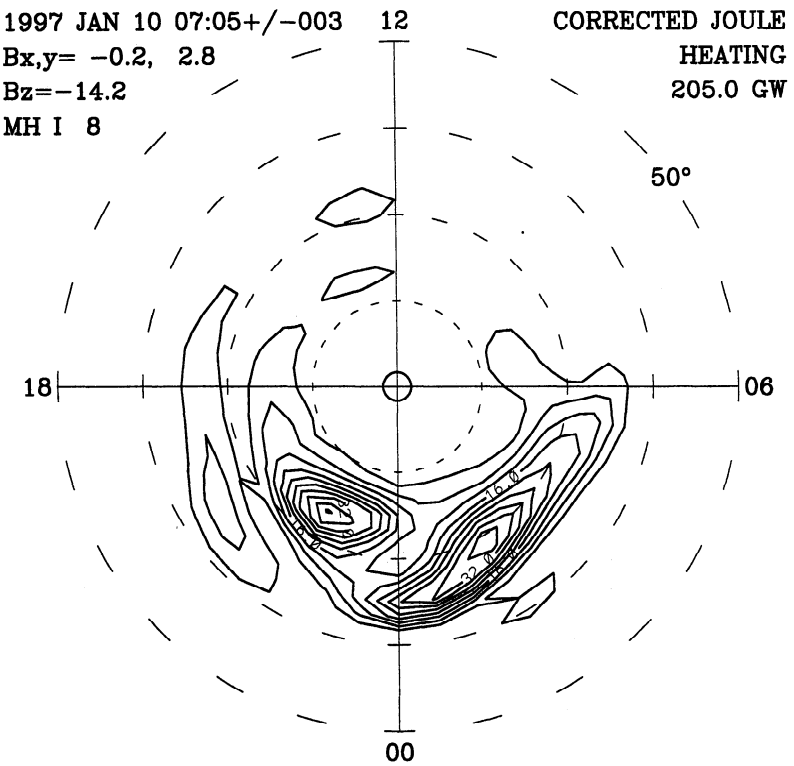

Figure 11. Northern Hemisphere Joule heating from AMIE for 0705 UT on January 10, 1997. The plot shows a peak in Joule heating at 70° N apex magnetic latitude at the longitudes of Millstone Hill and Arecibo. Units are 10^{-3} W m^{-2}.

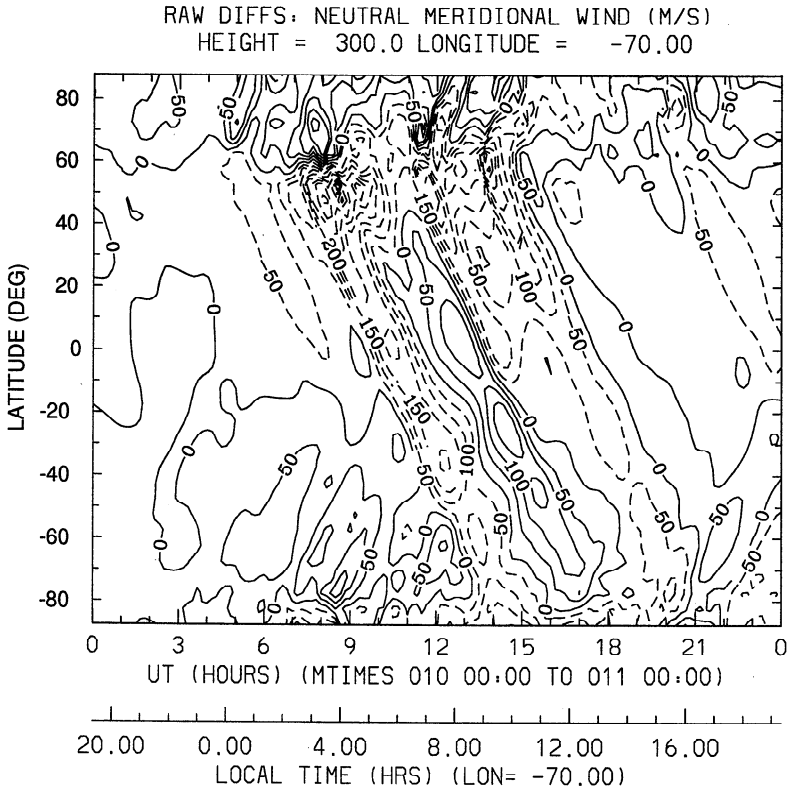

Figure 12. Neutral meridional wind perturbations from the TIEGCM for January 10, 1997, at an altitude of 300 km, showing TADs propagating equatorward from high-latitude source regions. Positive is toward geographic north.

found in the TIEGCM wind results for the disturbed night of November 4, 1993, by *Emery et al.* [1999]. In the TIEGCM, the wind surge which maximized at Millstone Hill at 0810 UT maximized at Arecibo at 0910 UT. This time lag gives a speed of propagation of 750 m s^{-1}, with the TAD launched from ~70° apex magnetic latitude (~60° geographic latitude) at ~0725 UT as shown in the Figure. However, the wind surge maximized ~45–50 min earlier in the Millstone Hill ISR data (~0720–0725 UT) and 40 min earlier in the servo model data (0730 UT) than in the TIEGCM, suggesting that the distribution of Joule heating and the speed of propagation of the TAD may be somewhat different than that given by the AMIE/TIEGCM. The times of the wind surge maxima observed by the Millstone Hill ISR and at Arecibo/Ramey give a speed of propagation of only 420 m s^{-1} and suggest the TAD was launched from 70° apex magnetic latitude at 0605 UT. Using the times of surge maxima given by the servo model at Millstone Hill and at Arecibo/Ramey gives a speed of propagation of 443 m s^{-1}, suggesting that the TAD was launched from 70° apex magnetic latitude at 0615 UT. Both of these times were before strong global Joule heating was seen by AMIE (Figure 3).

Richmond and Matsushita [1975] found a speed of propagation of 750 m s^{-1} for a large-scale atmospheric gravity wave (AGW) in their theoretical simulation of the response of the thermosphere to an isolated magnetic substorm. *Rice et al.* [1988] reported observations of a TAD seen at Millstone Hill with similar characteristics to the one discussed here. The horizontal speed was 718 m s^{-1}, the period 85 min, and the horizontal wavelength 3450 km. However, *Ho et al.* [1998] reported observations of a daytime TAD with a horizontal speed of only 460 m s^{-1} during the November 26, 1994 storm, and *Buonsanto et al.* [1999] reported observations of a 500 m s^{-1} daytime TAD during the May 2–5, 1995 storm. According to *Hocke and Schlegel* [1996], large-scale AGWs/TIDs propagate in the thermosphere with horizontal velocities between 400 and 1000 m s^{-1}. Sondrestrom (at 73.5° apex latitude) observed a brief period of Joule heating intensification centered at 0730 UT, consistent with the AMIE/TIEGCM estimates, and a much stronger interval of Joule heating centered at ~0825 UT [*Sanchez et al.*, 1998]. At 0615 UT, combined radar and optical data at Sondrestrom (not shown) shows that station near the poleward boundary of the auroral oval. Just inside the poleward boundary of the oval strong heating may occur in response to large fluxes of boundary plasma sheet electrons which cause discrete arcs [*Winningham et al.*, 1975]. More recently, *Innis et al.* [1997] have found a strong correlation between upward vertical winds and the poleward edge of the discrete auroral oval. Such large vertical winds are likely to be associated with heating events which can launch TADs.

6. Conclusion

Our combined analysis of the Sondrestrom, Millstone Hill, and Arecibo ISR data for the January 1997 storm provides observational evidence of TADs and of electric fields of magnetospheric origin penetrating from high to low latitude. We have been unsuccessful in isolating the precise time and location of the high-latitude source for a strong TAD observed by the Millstone and Arecibo ISRs from the data and modeling resources at hand. However, the good agreement between the data and TIEGCM at Arecibo, including the reproduction by the model of the timing of several observed fluctuations in hmF_2 and the meridional wind shows that we are clearly approaching the time when global models such as the TIEGCM,

driven by realistic high-latitude inputs, will be able to reproduce the actual sources and timing of TADs during storms. A greater challenge for the theoretical models as they develop further will be to reproduce the penetration of electric fields from high to low latitude. As this study and previous work shows, electric field penetration is a routine feature of the global response to geomagnetic storms. While the first of the two penetration events we identified may have been triggered by a change in the IMF, the second event was not, implying that more work needs to be done to clarify the relationship between IMF changes and electric field penetration to low latitude. While the TIEGCM reproduces many features of both the quiet and disturbed electron densities, further improvement is needed. This will require not only accurate magnetospheric and solar EUV energy inputs, but more data on the global neutral thermosphere compositional and dynamical response to geomagnetic activity. Such data are far too scarce at present, but validation of the model outputs by comparison with these kinds of data is needed to accelerate progress toward a reliable predictive capability.

Acknowledgments. We are grateful to B. A. Emery, P. J. Erickson, J. C. Foster, and two anonymous referees for useful comments. Millstone Hill data were acquired and analyzed under the support of a cooperative agreement between the National Science Foundation (NSF) and the Massachusetts Institute of Technology (MIT) and NSF grants ATM-9523673 and ATM-9813693 to MIT. Sondrestrom and Arecibo data were obtained from the CEDAR Database at the National Center for Atmospheric Research, Boulder, Colorado, which is supported by NSF. The Sondrestrom incoherent scatter radar is also supported by the NSF. The Arecibo Observatory is part of the National Astronomy and Ionosphere Center, which is operated by Cornell University with support from a cooperative agreement with the NSF. Wind solar wind velocity and plasma density data were supplied by the MIT Space Plasma Physics Group. Wind magnetic field data were obtained from the National Aeronautics and Space Administration (NASA) Wind Magnetic Field Investigation (MFI) World Wide Web site (R. P. Lepping, Principal Investigator). The equatorial *Dst* data were obtained from World Data Center C2 for Geomagnetism in Kyoto. The Millstone Hill and Ramey Digisonde data were provided by the University of Massachusetts Lowell Center for Atmospheric Research. B. W. Reinisch was supported by U.S. Air Force Contract F19628-96-C-0159.

Janet G. Luhmann thanks Alan Rodger and Nicola J. Fox for their assistance in evaluating this paper.

References

Alcayde, D., J. Fontanari, and P. Bauer, High latitude neutral atmosphere temperature and concentration measurements from the first Eiscat incoherent scatter observations, *Ann. Geophys.*, *38*, 473–480, 1982.

Babcock, R. R., Jr., and J. V. Evans, Effects of geomagnetic disturbances on neutral winds and temperatures in the thermosphere observed over Millstone Hill, *J. Geophys. Res.*, *84*, 5349–5354, 1979.

Bauer, P., P. Waldteufel, and D. Alcayde, Diurnal variations of the atomic oxygen density and temperature determined from incoherent scatter measurements in the ionospheric *F* region, *J. Geophys. Res.*, *75*, 4825–4832, 1970.

Buonsanto, M. J., Seasonal variations of day-time ionisation flows inferred from a comparison of calculated and observed NmF_2, *J. Atmos. Terr. Phys.*, *48*, 365–373, 1986.

Buonsanto, M. J., Millstone Hill incoherent scatter *F*-region observations during the disturbances of June 1991, *J. Geophys. Res.*, *100*, 5743–5755, 1995.

Buonsanto, M. J., and J. C. Foster, Effects of magnetospheric electric fields and neutral winds on the low-middle latitude ionosphere during the March 20–21, 1990 storm. *J. Geophys. Res.*, *98*, 19,133–19,140, 1993.

Buonsanto, M. J., and L. M. Pohlman, Climatology of neutral exospheric temperature above Millstone Hill, *J. Geophys. Res.*, *103*, 23,381–23,392, 1998.

Buonsanto, M. J., J. C. Foster, and D. P. Sipler, Observations from Millstone Hill during the geomagnetic disturbances of March and April, 1990, *J. Geophys. Res.*, *97*, 1225–1243, 1992.

Buonsanto, M. J., M. Codrescu, B. A. Emery, C. G. Fesen, T. J. Fuller-Rowell, D. J. Melendez-Alvira, and D. P. Sipler, Comparison of models and measurements at Millstone Hill during the January 24–26, 1993 minor storm interval, *J. Geophys. Res*, *102*, 7267–7277, 1997a.

Buonsanto, M. J., et al., Recent results of the CEDAR Storm Study, *Adv. Space Res.*, *20*(9), 1655–1664, 1997b.

Buonsanto, M. J., M. J. Starks, J. E. Titheridge, P. G. Richards, and K. L. Miller, Comparison of techniques for derivation of neutral meridional winds from ionospheric data, *J. Geophys. Res.*, *102*, 14,477–14,484, 1997c.

Buonsanto, M. J., S. González, X. Pi, J. M. Ruohoniemi, M. Sulzer, W. Swartz, J. Thayer, and D. N. Yuan, Radar chain study of the May, 1995 storm, *J. Atmos. Terr. Phys.*, *61*, 233–248, 1999.

Chen, C.-F., Critical analysis of ionogram profile inversions and comparison with incoherent scatter radar profiles, Ph.D. thesis, Univ. of Mass. Lowell, 1997.

Chen, C.-F., B. W. Reinisch, J. L. Scali, X. Huang, R. R. Gamache, M. J. Buonsanto, and B. D. Ward, The accuracy of ionogram-derived N(h) profiles, *Adv. Space Res.*, *14*(12), 43–46, 1994.

Coffey, H. E. (Ed.), *Solar Geophysical Data Prompt Reports, 631*, Part 1, pp. 109, National Geophysical Data Center, Boulder, Colo., 1997.

Cole, K. D., Stable auroral red arcs, sinks for energy of *Dst* main phase, *J. Geophys. Res.*, *70*, 1689–1706, 1965.

Crary, D. J., and J. M. Forbes, The dynamic ionosphere over Arecibo: A theoretical investigation, *J. Geophys. Res.*, *91*, 249–258, 1986.

Emery, B. A., C. Lathuillere, P. G. Richards, R. G. Roble, M. J. Buonsanto, D. J. Knipp, P. Wilkinson, D. P. Sipler, and R. Niciejewski, Time dependent thermospheric neutral response to the 2–11 November 1993 storm period, *J. Atmos. Solar. Terr. Phys.*, *61*, 329–350, 1999.

Evans, J. V., Midlatitude *F*-region densities and temperatures at sunspot minimum, *Planet. Space Sci.*, *15*, 1387–1405, 1967.

Farrugia, C. J., et al., Geoeffectiveness of three Wind magnetic clouds: A comparative study, *J. Geophys. Res.*, *103*, 17,261–17,268, 1998.

Fejer, B. G., The electrodynamics of the low-latitude ionosphere: recent results and future challenges, *J. Atmos. Sol. Terr. Phys.*, *59*, 1465–1482, 1997.

Fejer, B. G., and L. Scherliess, Time dependent response of equatorial ionospheric electric fields to magnetospheric disturbances, *Geophys. Res. Lett.*, *22*, 851–854, 1995.

Fejer, B. G., et al., Low- and mid-latitude ionospheric electric fields during the January 1984 GISMOS campaign, *J. Geophys. Res*, *95*, 2367–2377, 1990a.

Fejer, B. G., R. W. Spiro, R. A. Wolf, and J. C. Foster, Latitudinal variation of perturbation electric fields during magnetically disturbed periods: 1986 SUNDIAL observations and model results, *Ann. Geophys.*, *8*, 441–454, 1990b.

Fesen, C. G., B. A. Emery, M. J. Buonsanto, Q. H. Zhou, and M. P. Sulzer, Simulations of the *F* region during the January 1993 10-day campaign, *J. Geophys. Res*, *102*, 7249–7265, 1997.

Field, P. R., and H. Rishbeth, The response of the ionospheric F_2-layer to geomagnetic activity: An analysis of worldwide data, *J. Atmos. Solar-Terr. Phys.*, *59*, 163–180, 1997.

Foster, J. C., P. J. Erickson, J. M. Holt, and F. J. Rich, Millstone Hill observations of the mid-latitude electron temperature enhancement during the January 10, 1997 storm (abstract), *Eos Trans. AGU, 78*(46), Fall Meet. Suppl., 520–521, 1997.

Fox, N. J, M. Peredo, and B. J. Thompson, Cradle to grave tracking of the January 6–11, 1997 Sun-Earth connection event, *Geophys. Res. Lett.*, *25*, 2461–2464, 1998.

Fuller-Rowell, T. J., M. V. Codrescu, R. J. Moffett, and S. Quegan, Response of the thermosphere and ionosphere to geomagnetic storms, *J. Geophys. Res.*, *99*, 3893–3914, 1994.

Fuller-Rowell, T. J., M. V. Codrescu, H. Rishbeth, R. J. Moffett, and S. Quegan, On the seasonal response of the thermosphere and ionosphere to geomagnetic storms, *J. Geophys. Res.*, *101*, 2343–2353, 1996.

Gonzales, C. A., M. C. Kelley, R. A. Behnke, J. F. Vickrey, R. Wand, and J. Holt, On the latitudinal variations of the ionospheric electric field during magnetospheric disturbances, *J. Geophys. Res.*, *88*, 9135–9144, 1983.

Ho, C. M., A. J. Mannucci, L. Sparks, X. Pi, U. J. Lindqwister, B. D. Wilson, B. A. Iijima, and M. J. Reyes, Ionospheric total electron content perturbations monitored by the GPS global network during two northern hemisphere winter storms, *J. Geophys. Res.*, *103*, 26,409–26,420, 1998.

Hocke, K., and K. Schlegel, A review of atmospheric gravity waves and travelling ionospheric disturbances: 1982–1995, *Ann. Geophys.*, *14*, 917–940, 1996.

Huang, X., and B. W. Reinisch, Vertical electron density profiles from the Digisonde network, *Adv. Space Res.*, *18* (6), 121–129, 1996.

Innis, J. L., P. L. Dyson, and P. A. Greet, Further observations of the ther-

mospheric vertical wind at the auroral oval/polar cap boundary, *J. Atmos. Sol. Terr. Phys., 59*, 2009–2022, 1997.

Kelley, M. C., and C. A. Miller, Mid-latitude thermospheric plasma physics and electrodynamics: A review, *J. Atmos. Sol. Terr. Phys., 59*, 1643–1654, 1997.

Kozyra, J. U., E. C. Shelley, R. H. Comfort, L. H. Brace, T. E. Cravens, and A. F. Nagy, The role of ring current O^+ in the formation of stable auroral red arcs, *J. Geophys. Res., 92*, 7487–7502, 1987.

Lu, G., et al., Global energy deposition during the January 1997 magnetic cloud event, *J. Geophys. Res, 103*, 11,685–11,694, 1998a.

Lu., G., X. Pi, A. D. Richmond, and R. G. Roble, Variations of total electron content during geomagnetic disturbances: A model/observation comparison, *Geophys. Res. Lett., 25*, 253–256, 1998b.

MacPherson, B., S. A. González, G. J. Bailey, R. J. Moffett, and M. P. Sulzer, The effects of meridional neutral winds on the O^+–H^+ transition altitude over Arecibo, *J. Geophys. Res., 103*, 29,183–29,198, 1998.

Mikhailov, A. V., and M. Förster, Some F_2-layer effects during the January 06–11, 1997 CEDAR storm period as observed with the Millstone Hill incoherent scatter facility, *J. Atmos. Sol. Terr. Phys., 61*, 249–261, 1999.

Pesnell, W. D., K. Omidvar, and W. R. Hoegy, Momentum transfer collision frequency of O^+-O, *Geophys. Res. Lett., 20*, 1343–1346, 1993.

Prölss, G. W., On explaining the local time variation of ionospheric storm effects, *Ann. Geophys., 11*, 1–9, 1993.

Reinisch, B. W., and X. Huang, Automatic calculation of electron density profiles from digital ionograms, 3, Processing of bottomside ionograms, *Radio Sci., 18*, 477–486, 1983.

Rice, D. D., R. D. Hunsucker, L. J. Lanzerotti, G. Crowley, P. J. S. Williams, J. D. Craven, and L. Frank, An observation of atmospheric gravity wave cause and effect during the October 1985 WAGS campaign, *Radio Sci., 23*, 919–930, 1988.

Richards, P. G., and P. J. Wilkinson, The ionosphere and thermosphere at southern midlatitudes during the November 1993 ionospheric storm: A comparison of measurement and modeling, *J. Geophys. Res., 103*, 9373–9389, 1998.

Richmond, A. D., and Y. Kamide, Mapping electrodynamic features of the high-latitude ionosphere from localized observations: Technique, *J. Geophys. Res., 93*, 5741–5759, 1988.

Richmond, A. D., and S. Matsushita, Thermospheric response to a magnetic substorm, *J. Geophys. Res., 80*, 2839–2850, 1975.

Richmond, A. D., et al., An empirical model of quiet-day ionospheric electric fields at middle and low latitudes, *J. Geophys. Res., 85*, 4658–4664, 1980.

Richmond, A. D., et al., Mapping electrodynamic features of the high-latitude ionosphere from localized observations: Combined incoherent-scatter radar and magnetometer measurements for January 18–19, 1984, *J. Geophys. Res., 93*, 5760–5776, 1988.

Richmond, A. D., E. C. Ridley, and R. G. Roble, A thermosphere/ionosphere general circulation model with coupled electrodynamics, *Geophys. Res. Lett., 19*, 601–604, 1992.

Rishbeth, H., The effect of winds on the ionospheric F_2-peak, *J. Atmos. Terr. Phys., 29*, 225–238, 1967.

Rishbeth, H., S. Ganguly, and J. C. G. Walker, Field-aligned and field-perpendicular velocities in the ionospheric F_2-layer, *J. Atmos. Terr. Phys., 40*, 767–784, 1978.

Rodger, A. S., G. L. Wrenn, and H. Rishbeth, Geomagnetic storms in the Antarctic *F*-region. II. Physical interpretation, *J. Atmos. Terr. Phys., 51*, 851–866, 1989.

Salah, J. E., and J. M. Holt, Midlatitude thermospheric winds from incoherent scatter radar and theory, *Radio Sci., 9*, 301–313, 1974.

Sanchez, E. R., J. P. Thayer, J. D. Kelly, and R. A. Doe, Energy transfer between the ionosphere and magnetosphere during the January 1997 CME event, *Geophys. Res. Lett., 25*, 2597–2600, 1998.

Sastri, J. H., H. N. R. Rao, and K. B. Ramesh, Response of equatorial ionosphere to the transit of interplanetary magnetic cloud of January 13–15, 1967. Transient disturbance in *F* region, *Planet. Space Sci., 40*, 519–534, 1992.

Titheridge, J. E., and M. J. Buonsanto, A comparison of northern and summer hemisphere TEC storm behaviour, *J. Atmos. Terr. Phys., 50*, 763–780, 1988.

Winningham, J. D., F. Yasuhara, S.-I. Akasofu, and W. J. Heikkila, The latitudinal morphology of 10-eV to 10-keV electron fluxes during magnetically quiet and disturbed times in the 2100–0300 MLT sector, *J. Geophys. Res., 80*, 3148–3171, 1975.

M. J. Buonsanto, Massachusetts Institute of Technology, Haystack Observatory, Westford, MA 01886. (mjb@haystack.mit.edu)

S. A. González, Arecibo Observatory, HC3 Box 53995, Arecibo, PR 00612. (sixto@naic.edu)

G. Lu, High Altitude Observatory, National Center for Atmospheric Research, Boulder, CO 80307. (ganglu@ucar.edu)

B. W. Reinisch, Center for Atmospheric Research, University of Massachusetts Lowell, 600 Suffolk Street, Lowell, MA 01854. (Bodo_Reinisch@uml.edu)

J. P. Thayer, Geoscience and Engineering Center, SRI International, Menlo Park, CA 94025. (thayer@sri.com)

(Received January 29, 1999; revised June 14, 1999;
accepted August 10, 1999.)